arXiv:1302.5058v1 [hep-ex] 20 Feb 2013

DESY–13–028
February 21, 2013

Measurement of $D^{\pm}$ production in deep inelastic ep scattering with the ZEUS detector at HERA

ZEUS Collaboration

Abstract

Charm production in deep inelastic ep scattering was measured with the ZEUS detector using an integrated luminosity of $354\,\mathrm{pb}^{-1}$. Charm quarks were identified by reconstructing $D^{\pm}$ mesons in the $D^{\pm} \to K^{\mp}\pi^{\pm}\pi^{\pm}$ decay channel. Lifetime information was used to reduce combinatorial background substantially. Differential cross sections were measured in the kinematic region $5 < Q^2 < 1000\,\mathrm{GeV}^2$, $0.02 < y < 0.7$, $1.5 < p_T(D^{\pm}) < 15\,\mathrm{GeV}$ and $|\eta(D^{\pm})| < 1.6$, where Q^2 is the photon virtuality, y is the inelasticity, and $p_T(D^{\pm})$ and $\eta(D^{\pm})$ are the transverse momentum and the pseudorapidity of the $D^{\pm}$ meson, respectively. Next-to-leading-order QCD predictions are compared to the data. The charm contribution, $F_2^{c\bar{c}}$, to the proton structure-function F_2 was extracted.

The ZEUS Collaboration

H. Abramowicz[45,aj], I. Abt[35], L. Adamczyk[13], M. Adamus[54], R. Aggarwal[7,c], S. Antonelli[4], P. Antonioli[3], A. Antonov[33], M. Arneodo[50], O. Arslan[5], V. Aushev[26,27,aa], Y. Aushev,[27,aa,ab], O. Bachynska[15], A. Bamberger[19], A.N. Barakbaev[25], G. Barbagli[17], G. Bari[3], F. Barreiro[30], N. Bartosik[15], D. Bartsch[5], M. Basile[4], O. Behnke[15], J. Behr[15], U. Behrens[15], L. Bellagamba[3], A. Bertolin[39], S. Bhadra[57], M. Bindi[4], C. Blohm[15], V. Bokhonov[26,aa], T. Bołd[13], E.G. Boos[25], K. Borras[15], D. Boscherini[3], D. Bot[15], I. Brock[5], E. Brownson[56], R. Brugnera[40], N. Brümmer[37], A. Bruni[3], G. Bruni[3], B. Brzozowska[53], P.J. Bussey[20], B. Bylsma[37], A. Caldwell[35], M. Capua[8], R. Carlin[40], C.D. Catterall[57], S. Chekanov[1], J. Chwastowski[12,e], J. Ciborowski[53,an], R. Ciesielski[15,h], L. Cifarelli[4], F. Cindolo[3], A. Contin[4], A.M. Cooper-Sarkar[38], N. Coppola[15,i], M. Corradi[3], F. Corriveau[31], M. Costa[49], G. D'Agostini[43], F. Dal Corso[39], J. del Peso[30], R.K. Dementiev[34], S. De Pasquale[4,a], M. Derrick[1], R.C.E. Devenish[38], D. Dobur[19,u], B.A. Dolgoshein [33,†], G. Dolinska[15], A.T. Doyle[20], V. Drugakov[16], L.S. Durkin[37], S. Dusini[39], Y. Eisenberg[55], P.F. Ermolov [34,†], A. Eskreys [12,†], S. Fang[15,j], S. Fazio[8], J. Ferrando[20], M.I. Ferrero[49], J. Figiel[12], B. Foster[38,af], G. Gach[13], A. Galas[12], E. Gallo[17], A. Garfagnini[40], A. Geiser[15], I. Gialas[21,x], A. Gizhko[15], L.K. Gladilin[34], D. Gladkov[33], C. Glasman[30], O. Gogota[27], Yu.A. Golubkov[34], P. Göttlicher[15,k], I. Grabowska-Bołd[13], J. Grebenyuk[15], I. Gregor[15], G. Grigorescu[36], G. Grzelak[53], O. Gueta[45], M. Guzik[13], C. Gwenlan[38,ag], T. Haas[15], W. Hain[15], R. Hamatsu[48], J.C. Hart[44], H. Hartmann[5], G. Hartner[57], E. Hilger[5], D. Hochman[55], R. Hori[47], A. Hüttmann[15], Z.A. Ibrahim[10], Y. Iga[42], R. Ingbir[45], M. Ishitsuka[46], A. Iudin[27,ac], H.-P. Jakob[5], F. Januschek[15], T.W. Jones[52], M. Jüngst[5], I. Kadenko[27], B. Kahle[15], S. Kananov[45], T. Kanno[46], U. Karshon[55], F. Karstens[19,v], I.I. Katkov[15,l], M. Kaur[7], P. Kaur[7,c], A. Keramidas[36], L.A. Khein[34], J.Y. Kim[9], D. Kisielewska[13], S. Kitamura[48,al], R. Klanner[22], U. Klein[15,m], E. Koffeman[36], N. Kondrashova[27,ad], O. Kononenko[27], P. Kooijman[36], Ie. Korol[15], I.A. Korzhavina[34], A. Kotański[14,f], U. Kötz[15], N. Kovalchuk[27,ae], H. Kowalski[15], O. Kuprash[15], M. Kuze[46], A. Lee[37], B.B. Levchenko[34], A. Levy[45], V. Libov[15], S. Limentani[40], T.Y. Ling[37], M. Lisovyi[15], E. Lobodzinska[15], W. Lohmann[16], B. Löhr[15], E. Lohrmann[22], K.R. Long[23], A. Longhin[39,ah], D. Lontkovskyi[15], O.Yu. Lukina[34], J. Maeda[46,ak], S. Magill[1], I. Makarenko[15], J. Malka[15], R. Mankel[15], A. Margotti[3], G. Marini[43], J.F. Martin[51], A. Mastroberardino[8], M.C.K. Mattingly[2], I.-A. Melzer-Pellmann[15], S. Mergelmeyer[5], S. Miglioranzi[15,n], F. Mohamad Idris[10], V. Monaco[49], A. Montanari[15], J.D. Morris[6,b], K. Mujkic[15,o], B. Musgrave[1], K. Nagano[24], T. Namsoo[15,p], R. Nania[3], A. Nigro[43], Y. Ning[11], T. Nobe[46], D. Notz[15], R.J. Nowak[53], A.E. Nuncio-Quiroz[5], B.Y. Oh[41], N. Okazaki[47], K. Olkiewicz[12], Yu. Onishchuk[27], K. Papageorgiu[21], A. Parenti[15], E. Paul[5], J.M. Pawlak[53], B. Pawlik[12], P. G. Pelfer[18], A. Pellegrino[36], W. Perlański[53,ao], H. Perrey[15], K. Piotrzkowski[29], P. Pluciński[54,ap], N.S. Pokrovskiy[25], A. Polini[3], A.S. Proskuryakov[34], M. Przybycień[13], A. Raval[15], D.D. Reeder[56], B. Reisert[35], Z. Ren[11], J. Repond[1], Y.D. Ri[48,am], A. Robertson[38], P. Roloff[15,n], I. Rubinsky[15], M. Ruspa[50], R. Sacchi[49], U. Samson[5], G. Sartorelli[4], A.A. Savin[56], D.H. Saxon[20], M. Schioppa[8], S. Schlenstedt[16], P. Schleper[22], W.B. Schmidke[35], U. Schneekloth[15], V. Schönberg[5], T. Schörner-Sadenius[15], J. Schwartz[31], F. Sciulli[11], L.M. Shcheglova[34], R. Shehzadi[5], S. Shimizu[47,n], I. Singh[7,c], I.O. Skillicorn[20], W. Słomiński[14,g], W.H. Smith[56], V. Sola[22], A. Solano[49], D. Son[28], V. Sosnovtsev[33], A. Spiridonov[15,q], H. Stadie[22], L. Stanco[39], N. Stefaniuk[27], A. Stern[45], T.P. Stewart[51], A. Stifutkin[33], P. Stopa[12], S. Suchkov[33], G. Susinno[8], L. Suszycki[13], J. Sztuk-

Dambietz[22], D. Szuba[22], J. Szuba[15,r], A.D. Tapper[23], E. Tassi[8,d], J. Terrón[30], T. Theedt[15], H. Tiecke[36], K. Tokushuku[24,y], J. Tomaszewska[15,s], A. Trofymov[27,ae], V. Trusov[27], T. Tsurugai[32], M. Turcato[22], O. Turkot[27,ae,t], T. Tymieniecka[54,aq], M. Vázquez[36,n], A. Verbytskyi[15], O. Viazlo[27], N.N. Vlasov[19,w], R. Walczak[38], W.A.T. Wan Abdullah[10], J.J. Whitmore[41,ai], K. Wichmann[15,t], L. Wiggers[36], M. Wing[52], M. Wlasenko[5], G. Wolf[15], H. Wolfe[56], K. Wrona[15], A.G. Yagües-Molina[15], S. Yamada[24], Y. Yamazaki[24,z], R. Yoshida[1], C. Youngman[15], N. Zakharchuk[27,ae], A.F. Żarnecki[53], L. Zawiejski[12], O. Zenaiev[15], W. Zeuner[15,n], B.O. Zhautykov[25], N. Zhmak[26,aa], A. Zichichi[4], Z. Zolkapli[10], D.S. Zotkin[34]

1 *Argonne National Laboratory, Argonne, Illinois 60439-4815, USA* [A]

2 *Andrews University, Berrien Springs, Michigan 49104-0380, USA*

3 *INFN Bologna, Bologna, Italy* [B]

4 *University and INFN Bologna, Bologna, Italy* [B]

5 *Physikalisches Institut der Universität Bonn, Bonn, Germany* [C]

6 *H.H. Wills Physics Laboratory, University of Bristol, Bristol, United Kingdom* [D]

7 *Panjab University, Department of Physics, Chandigarh, India*

8 *Calabria University, Physics Department and INFN, Cosenza, Italy* [B]

9 *Institute for Universe and Elementary Particles, Chonnam National University, Kwangju, South Korea*

10 *Jabatan Fizik, Universiti Malaya, 50603 Kuala Lumpur, Malaysia* [E]

11 *Nevis Laboratories, Columbia University, Irvington on Hudson, New York 10027, USA* [F]

12 *The Henryk Niewodniczanski Institute of Nuclear Physics, Polish Academy of Sciences, Krakow, Poland* [G]

13 *AGH-University of Science and Technology, Faculty of Physics and Applied Computer Science, Krakow, Poland* [H]

14 *Department of Physics, Jagellonian University, Cracow, Poland*

15 *Deutsches Elektronen-Synchrotron DESY, Hamburg, Germany*

16 *Deutsches Elektronen-Synchrotron DESY, Zeuthen, Germany*

17 *INFN Florence, Florence, Italy* [B]

18 *University and INFN Florence, Florence, Italy* [B]

19 *Fakultät für Physik der Universität Freiburg i.Br., Freiburg i.Br., Germany*

20 *School of Physics and Astronomy, University of Glasgow, Glasgow, United Kingdom* [D]

21 *Department of Engineering in Management and Finance, Univ. of the Aegean, Chios, Greece*

22 *Hamburg University, Institute of Experimental Physics, Hamburg, Germany* [I]

23 *Imperial College London, High Energy Nuclear Physics Group, London, United Kingdom* [D]

24 *Institute of Particle and Nuclear Studies, KEK, Tsukuba, Japan* [J]

25 *Institute of Physics and Technology of Ministry of Education and Science of Kazakhstan, Almaty, Kazakhstan*

26 *Institute for Nuclear Research, National Academy of Sciences, Kyiv, Ukraine*

27 *Department of Nuclear Physics, National Taras Shevchenko University of Kyiv, Kyiv, Ukraine*

28 *Kyungpook National University, Center for High Energy Physics, Daegu, South Korea* [K]

29 *Institut de Physique Nucléaire, Université Catholique de Louvain, Louvain-la-Neuve, Belgium* [L]

30 *Departamento de Física Teórica, Universidad Autónoma de Madrid, Madrid, Spain* [M]

31 *Department of Physics, McGill University, Montréal, Québec, Canada H3A 2T8* [N]

32 *Meiji Gakuin University, Faculty of General Education, Yokohama, Japan* [J]

[33] *Moscow Engineering Physics Institute, Moscow, Russia* [O]
[34] *Lomonosov Moscow State University, Skobeltsyn Institute of Nuclear Physics, Moscow, Russia* [P]
[35] *Max-Planck-Institut für Physik, München, Germany*
[36] *NIKHEF and University of Amsterdam, Amsterdam, Netherlands* [Q]
[37] *Physics Department, Ohio State University, Columbus, Ohio 43210, USA* [A]
[38] *Department of Physics, University of Oxford, Oxford, United Kingdom* [D]
[39] *INFN Padova, Padova, Italy* [B]
[40] *Dipartimento di Fisica dell' Università and INFN, Padova, Italy* [B]
[41] *Department of Physics, Pennsylvania State University, University Park, Pennsylvania 16802, USA* [F]
[42] *Polytechnic University, Tokyo, Japan* [J]
[43] *Dipartimento di Fisica, Università 'La Sapienza' and INFN, Rome, Italy* [B]
[44] *Rutherford Appleton Laboratory, Chilton, Didcot, Oxon, United Kingdom* [D]
[45] *Raymond and Beverly Sackler Faculty of Exact Sciences, School of Physics, Tel Aviv University, Tel Aviv, Israel* [R]
[46] *Department of Physics, Tokyo Institute of Technology, Tokyo, Japan* [J]
[47] *Department of Physics, University of Tokyo, Tokyo, Japan* [J]
[48] *Tokyo Metropolitan University, Department of Physics, Tokyo, Japan* [J]
[49] *Università di Torino and INFN, Torino, Italy* [B]
[50] *Università del Piemonte Orientale, Novara, and INFN, Torino, Italy* [B]
[51] *Department of Physics, University of Toronto, Toronto, Ontario, Canada M5S 1A7* [N]
[52] *Physics and Astronomy Department, University College London, London, United Kingdom* [D]
[53] *Faculty of Physics, University of Warsaw, Warsaw, Poland*
[54] *National Centre for Nuclear Research, Warsaw, Poland*
[55] *Department of Particle Physics and Astrophysics, Weizmann Institute, Rehovot, Israel*
[56] *Department of Physics, University of Wisconsin, Madison, Wisconsin 53706, USA* [A]
[57] *Department of Physics, York University, Ontario, Canada M3J 1P3* [N]

[A] supported by the US Department of Energy
[B] supported by the Italian National Institute for Nuclear Physics (INFN)
[C] supported by the German Federal Ministry for Education and Research (BMBF), under contract No. 05 H09PDF
[D] supported by the Science and Technology Facilities Council, UK
[E] supported by HIR and UMRG grants from Universiti Malaya, and an ERGS grant from the Malaysian Ministry for Higher Education
[F] supported by the US National Science Foundation. Any opinion, findings and conclusions or recommendations expressed in this material are those of the authors and do not necessarily reflect the views of the National Science Foundation.
[G] supported by the Polish Ministry of Science and Higher Education as a scientific project No. DPN/N188/DESY/2009
[H] supported by the Polish Ministry of Science and Higher Education and its grants for Scientific Research
[I] supported by the German Federal Ministry for Education and Research (BMBF), under contract No. 05h09GUF, and the SFB 676 of the Deutsche Forschungsgemeinschaft (DFG)
[J] supported by the Japanese Ministry of Education, Culture, Sports, Science and Technology (MEXT) and its grants for Scientific Research
[K] supported by the Korean Ministry of Education and Korea Science and Engineering Foundation
[L] supported by FNRS and its associated funds (IISN and FRIA) and by an Inter-University Attraction Poles Programme subsidised by the Belgian Federal Science Policy Office
[M] supported by the Spanish Ministry of Education and Science through funds provided by CICYT
[N] supported by the Natural Sciences and Engineering Research Council of Canada (NSERC)
[O] partially supported by the German Federal Ministry for Education and Research (BMBF)
[P] supported by RF Presidential grant N 3920.2012.2 for the Leading Scientific Schools and by the Russian Ministry of Education and Science through its grant for Scientific Research on High Energy Physics
[Q] supported by the Netherlands Foundation for Research on Matter (FOM)
[R] supported by the Israel Science Foundation

[a] now at University of Salerno, Italy
[b] now at Queen Mary University of London, United Kingdom
[c] also funded by Max Planck Institute for Physics, Munich, Germany
[d] also Senior Alexander von Humboldt Research Fellow at Hamburg University, Institute of Experimental Physics, Hamburg, Germany
[e] also at Cracow University of Technology, Faculty of Physics, Mathematics and Applied Computer Science, Poland
[f] supported by the research grant No. 1 P03B 04529 (2005-2008)
[g] partially supported by the Polish National Science Centre projects DEC-2011/01/B/ST2/03643 and DEC-2011/03/B/ST2/00220
[h] now at Rockefeller University, New York, NY 10065, USA
[i] now at DESY group FS-CFEL-1
[j] now at Institute of High Energy Physics, Beijing, China
[k] now at DESY group FEB, Hamburg, Germany
[l] also at Moscow State University, Russia
[m] now at University of Liverpool, United Kingdom
[n] now at CERN, Geneva, Switzerland
[o] also affiliated with University College London, UK
[p] now at Goldman Sachs, London, UK
[q] also at Institute of Theoretical and Experimental Physics, Moscow, Russia
[r] also at FPACS, AGH-UST, Cracow, Poland
[s] partially supported by Warsaw University, Poland
[t] supported by the Alexander von Humboldt Foundation
[u] now at Istituto Nazionale di Fisica Nucleare (INFN), Pisa, Italy
[v] now at Haase Energie Technik AG, Neumünster, Germany
[w] now at Department of Physics, University of Bonn, Germany
[x] also affiliated with DESY, Germany
[y] also at University of Tokyo, Japan
[z] now at Kobe University, Japan
[†] deceased
[aa] supported by DESY, Germany
[ab] member of National Technical University of Ukraine, Kyiv Polytechnic Institute, Kyiv, Ukraine
[ac] member of National Technical University of Ukraine, Kyiv, Ukraine
[ad] now at DESY ATLAS group
[ae] member of National University of Kyiv - Mohyla Academy, Kyiv, Ukraine
[af] Alexander von Humboldt Professor; also at DESY and University of Oxford
[ag] STFC Advanced Fellow
[ah] now at LNF, Frascati, Italy
[ai] This material was based on work supported by the National Science Foundation, while working at the Foundation.
[aj] also at Max Planck Institute for Physics, Munich, Germany, External Scientific Member

[ak] now at Tokyo Metropolitan University, Japan
[al] now at Nihon Institute of Medical Science, Japan
[am] now at Osaka University, Osaka, Japan
[an] also at Łódź University, Poland
[ao] member of Łódź University, Poland
[ap] now at Department of Physics, Stockholm University, Stockholm, Sweden
[aq] also at Cardinal Stefan Wyszyński University, Warsaw, Poland

1 Introduction

Measurements of charm production in deep inelastic ep scattering (DIS) at HERA provide powerful constraints on the proton structure. The dominant production mechanism, the boson-gluon fusion (BGF) process, $\gamma g \to c\bar{c}$, provides direct access to the gluon content of the proton. As charm-quark production contributes up to 30% of the inclusive DIS cross sections at HERA, a correct modelling of this contribution in perturbative QCD (pQCD) calculations is important for determining parton distribution functions (PDFs) of the proton. One crucial issue is the treatment of charm-quark mass effects.

At HERA, several different charm-tagging techniques have been exploited to measure charm production in DIS [1–12]. Recently, a combined analysis of these data was performed [13], yielding results with both statistical and systematic uncertainties significantly reduced. In general, perturbative QCD predictions at next-to-leading order (NLO) are in reasonable agreement with the measurements. These data have also been used to obtain a precise determination of the charm-quark mass [13, 14].

In the analysis presented here, a charm quark in the final state was identified by the presence of a D^+ meson[1], using the $D^+ \to K^-\pi^+\pi^+$ decay. The lifetime of D^+ mesons was used to suppress combinatorial background by reconstructing the corresponding secondary vertex. All data available after the HERA luminosity upgrade were used and this publication supersedes a previous one [3] which was based on a subset of the data. Three times more data were analysed for the current paper, with better control of the systematic uncertainties.

Differential cross sections were measured as a function of the photon virtuality at the electron vertex, Q^2, the inelasticity, y, and the transverse momentum, $p_T(D^+)$, and pseudorapidity, $\eta(D^+)$, of the D^+ meson . The charm contribution to the proton structure-function F_2, denoted as $F_2^{c\bar{c}}$, was extracted from the double-differential cross sections in Q^2 and y. Previous measurements, as well as NLO QCD predictions, are compared to the data.

2 Experimental set-up

The analysis was performed with data taken from 2004 to 2007, when HERA collided electrons or positrons with energy $E_e = 27.5\,\text{GeV}$ and protons with $E_p = 920\,\text{GeV}$, corresponding to a centre-of-mass energy $\sqrt{s} = 318\,\text{GeV}$. The corresponding integrated luminosity was $\mathcal{L} = 354 \pm 7\,\text{pb}^{-1}$.

[1] Charge-conjugate modes are implied throughout the paper.

A detailed description of the ZEUS detector can be found elsewhere [15]. A brief outline of the components that are most relevant for this analysis is given below.

In the kinematic range of the analysis, charged particles were tracked in the central tracking detector (CTD) [16] and the microvertex detector (MVD) [17]. These components operated in a magnetic field of 1.43 T provided by a thin superconducting solenoid. The CTD consisted of 72 cylindrical drift-chamber layers, organised in nine superlayers covering the polar-angle[2] region $15^\circ < \theta < 164^\circ$. The MVD silicon tracker consisted of a barrel (BMVD) and a forward (FMVD) section. The BMVD contained three layers and provided polar-angle coverage for tracks from 30° to 150°. The four-layer FMVD extended the polar-angle coverage in the forward region to 7°. After alignment, the single-hit resolution of the MVD was 24 μm. The transverse distance of closest approach (DCA) of tracks to the nominal vertex in XY was measured to have a resolution, averaged over the azimuthal angle, of $(46 \oplus 122/p_T)$ μm, with p_T in GeV. For CTD-MVD tracks that pass through all nine CTD superlayers, the momentum resolution was $\sigma(p_T)/p_T = 0.0029 p_T \oplus 0.0081 \oplus 0.0012/p_T$, with p_T in GeV.

The high-resolution uranium–scintillator calorimeter (CAL) [18] consisted of three parts: the forward (FCAL), the barrel (BCAL) and the rear (RCAL) calorimeters. Each part was subdivided transversely into towers and longitudinally into one electromagnetic section (EMC) and either one (in RCAL) or two (in BCAL and FCAL) hadronic sections (HAC). The smallest subdivision of the calorimeter is called a cell. The CAL energy resolutions, as measured under test-beam conditions, are $\sigma(E)/E = 0.18/\sqrt{E}$ for electrons and $\sigma(E)/E = 0.35/\sqrt{E}$ for hadrons, with E in GeV.

The luminosity was measured using the Bethe-Heitler reaction $ep \to e\gamma p$ by a luminosity detector which consisted of independent lead–scintillator calorimeter [19] and magnetic spectrometer [20] systems. The fractional systematic uncertainty on the measured luminosity was 1.9%.

3 Theoretical predictions

Charm production in DIS has been calculated at NLO ($\mathcal{O}(\alpha_s^2)$) in the so-called fixed-flavour-number scheme (FFNS) [21], in which the proton contains only light flavours and heavy quarks are produced in the hard interaction.

[2] The ZEUS coordinate system is a right-handed Cartesian system, with the Z axis pointing in the proton beam direction, referred to as the "forward direction", and the X axis pointing towards the centre of HERA. The coordinate origin is at the nominal interaction point. The pseudorapidity is defined as $\eta = -\ln\left(\tan\frac{\theta}{2}\right)$, where the polar angle, θ, is measured with respect to the proton beam direction.

The HVQDIS program [22] has been used to calculate QCD predictions for comparison to the results of this analysis, as well as to extrapolate the measured visible cross sections to obtain $F_2^{c\bar{c}}$. The renormalisation and factorisation scales were set to $\mu_R = \mu_F = \sqrt{Q^2 + 4m_c^2}$ and the charm-quark pole mass to $m_c = 1.5\,\text{GeV}$. The FFNS variant of the ZEUS-S NLO QCD PDF fit [23] to inclusive structure-function data was used as the parametrisation of the proton PDFs. The same charm mass and choice of scales was used in the fit as in the HVQDIS calculation. The value of $\alpha_s(M_Z)$ in the three-flavour FFNS was set to 0.105, corresponding to $\alpha_s(M_Z) = 0.116$ in the five-flavour scheme.

To calculate D^+ observables, events at the parton level were interfaced with a fragmentation model based on the Kartvelishvili function [24]. The fragmentation was performed in the $\gamma^* p$ centre-of-mass frame. The Kartvelishvili parameter, α, was parametrised [25] as a smooth function of the invariant mass of the $c\bar{c}$ system, $M_{c\bar{c}}$, to fit the measurements of the D^* fragmentation function by ZEUS [26] and H1 [27]: $\alpha(M_{c\bar{c}}) = 2.1 + 127/(M_{c\bar{c}}^2 - 4m_c^2)$ (with m_c and $M_{c\bar{c}}$ in GeV). In addition, the mean value of the fragmentation function was scaled down by 0.95 since kinematic considerations [28] and direct measurements at Belle [29] and CLEO [30] show that, on average, the momentum of D^+ mesons is 5% lower than that of D^* mesons. This is due to some of the D^+ mesons originating from D^* decays. For the hadronisation fraction, $f(c \to D^+)$, the value 0.2297 ± 0.0078 was used [31], having corrected the branching ratios to those in the PDG 2012 [32].

The uncertainties on the theoretical predictions were estimated as follows:

- the renormalisation and factorisation scales were independently varied up and down by a factor 2;
- the charm-quark mass was consistently changed in the PDF fits and in the HVQDIS calculations by $\pm 0.15\,\text{GeV}$;
- the proton PDFs were varied within the total uncertainties of the ZEUS-S PDF fit;
- the fragmentation function was varied by changing the functional dependence of the parametrisation function $\alpha(M_{c\bar{c}})$ within uncertainties [25];
- the hadronisation fraction was varied within its uncertainties.

The total theoretical uncertainty was obtained by summing in quadrature the effects of the individual variations. The dominant contributions originate from the variations of the charm-quark mass and the scales. In previous studies [13] the uncertainty due to the variation of $\alpha_s(M_Z)$ was found to be insignificant and therefore it was neglected here.

A second NLO calculation was used in this analysis. It is based on the general-mass variable-flavour-number scheme (GM-VFNS) [33]. In this scheme, charm production is treated in the FFNS in the low-Q^2 region, where the mass effects are largest, and in the zero-mass variable-flavour-number scheme (ZM-VFNS) [34] at high Q^2. In the ZM-VFNS,

the charm-quark mass is set to zero in the computation of the matrix elements and the kinematics. Charm is treated as an active flavour in the proton above the kinematic threshold, $Q^2 \approx m_c^2$. At intermediate scales, an interpolation is made in the GM-VFNS between the FFNS and the ZM-VFNS, avoiding double counting of common terms.

4 Monte Carlo samples

Monte Carlo (MC) simulations were used to determine detector acceptances and to estimate and subtract the contributions of D^+ mesons originating from beauty decays. The MC events were generated with the RAPGAP 3.00 [35] program, interfaced with HERACLES 4.6.1 [36] to incorporate first-order electroweak corrections. The RAPGAP generator uses the leading-order matrix element for the charm and beauty BGF process and parton showers to simulate higher-order QCD effects. The CTEQ5L [37] PDFs were used for the proton. The heavy-quark masses were set to $m_c = 1.5\,\text{GeV}$ and $m_b = 4.75\,\text{GeV}$. The heavy-quark fragmentation was modelled using the Lund string model with the Bowler modifications for the longitudinal component [38].

The generated events were passed through a full simulation of the ZEUS detector based on GEANT 3.21 [39]. They had then to fulfil the same trigger criteria and pass the same reconstruction programs as the data.

5 Selection of DIS events

A three-level trigger system [15, 40] was used to select DIS events online. Most of the first-level triggers (FLTs) used in this analysis had some requirements on the track multiplicity in the events. The efficiency of these criteria was measured using a trigger without track requirements and the detector simulation was tuned to match the data. The trigger-inefficiency corrections for the simulation were between $1-10\%$ for different tracking requirements. The corrections changed the overall efficiency of the triggers used in the analysis [25] by a negligible amount for medium-Q^2 values and up to $\approx 2\%$ for the low- and high-Q^2 regions. At the third trigger level, DIS events were selected by requiring a scattered electron to be detected in the CAL.

The kinematic variables Q^2 and y were reconstructed offline using the double-angle (DA) method [41], which relies on the angles of the scattered electron and the hadronic final state. To select a clean DIS sample the following cuts were applied:

- $E_{e'} > 10\,\text{GeV}$, where $E_{e'}$ is the energy of the reconstructed scattered electron;

- $E^{\mathrm{cone}}_{\mathrm{non}\,e'} < 5\,\mathrm{GeV}$, where $E^{\mathrm{cone}}_{\mathrm{non}\,e'}$ is the energy deposit in the CAL in a cone around the electron candidate, not originating from it. The cone was defined by the criterion $\sqrt{\Delta\eta^2 + \Delta\phi^2} < 0.8$, where ϕ is the azimuthal angle;
- for scattered electrons detected in the RCAL, the impact point of the candidate on the surface of the RCAL was required to lie outside a rectangular region ($\pm 13\,\mathrm{cm}$ in X and $\pm 13\,\mathrm{cm}$ in Y) centred on the origin of coordinates;
- $40 < \delta < 65\,\mathrm{GeV}$, where $\delta = \sum_i E_i(1 - \cos\theta_i)$ and E_i and θ_i are the energy and the polar angle of the i^{th} energy-flow object (EFO) [42] reconstructed from CTD+MVD tracks and energy clusters measured in the CAL. This cut was imposed to select fully contained neutral-current ep events, for which $\delta = 2E_e = 55\,\mathrm{GeV}$ and to suppress photoproduction contamination and cosmic-ray background;
- $|Z_{\mathrm{vtx}}| < 30\,\mathrm{cm}$, where Z_{vtx} is the Z position of the primary vertex;
- $y_{\mathrm{JB}} > 0.02$, where y was reconstructed using the Jacquet-Blondel method [43].

The selected kinematic region was $5 < Q^2_{\mathrm{DA}} < 1000\,\mathrm{GeV}^2$ and $0.02 < y_{\mathrm{DA}} < 0.7$.

6 Reconstruction of D^+ mesons

The D^+ mesons were reconstructed using the decay channel $D^+ \to K^-\pi^+\pi^+$. In each event, track pairs with equal charges were combined with a third track with the opposite charge to form D^+ candidates. The pion mass was assigned to the tracks with equal charges and the kaon mass was assigned to the remaining track. The three tracks were then fitted to a common vertex and the invariant mass, $M(K\pi\pi)$, was calculated. The tracks were required to have a transverse momentum $p_T(K) > 0.5\,\mathrm{GeV}$ and $p_T(\pi) > 0.35\,\mathrm{GeV}$, respectively. To ensure high momentum and position resolution, all tracks were required to be reconstructed within $|\eta| < 1.75$, to have passed through at least three superlayers of the CTD and to have at least two BMVD hits in the XY plane and two in the Z direction. A special study [44] was performed to assess the tracking inefficiency for charged pions due to hadronic interactions in the detector material and how well the MC reproduces these interactions. The MC simulation was found to underestimate the interaction rate by about 40% for $p_T < 1.5\,\mathrm{GeV}$ and to agree with the data for $p_T > 1.5\,\mathrm{GeV}$. A corresponding correction was applied to the MC. The effect of the correction on the D^+ production cross section was about 3%.

The kinematic region for D^+ candidates was $1.5 < p_T(D^+) < 15\,\mathrm{GeV}$ and $|\eta(D^+)| < 1.6$. The contribution from $D^{*+} \to D^0\pi^+ \to K^-\pi^+\pi^+$ was suppressed by removing combinations with $M(K\pi\pi) - M(K\pi) < 0.15\,\mathrm{GeV}$. A small contribution from $D_s^+ \to \phi\pi^+ \to K^-K^+\pi^+$ was suppressed by assuming one of the pions to be a kaon and requiring the

invariant mass of the kaon pair to lie outside the ϕ mass peak region $1.0115 < M(KK) < 1.0275\,\mathrm{GeV}$. A remaining reflection from $D_s^+ \to K^-K^+\pi^+$ decays without intermediate ϕ production was estimated using the RAPGAP MC sample. It was found to be $\approx 1\%$ and was subtracted from the mass distribution.

A powerful discriminating variable to suppress combinatorial background originating from light-flavour production is the decay-length significance, S_l. It is defined as $S_l = l/\sigma_l$, where l is the decay length in the transverse plane, projected on to the D^+ meson momentum, and σ_l is the uncertainty associated with this distance. The decay length itself was determined as the distance in XY between the secondary vertex fitted in 3D and the interaction point. In the XY plane, the interaction point is defined as the position of the primary vertex determined from selected tracks and using the beam-spot position [3] as an additional constraint. The widths of the beam spot were 88 µm (80 µm) and 24 µm (22 µm) in the X and Y directions, respectively, for the e^+p (e^-p) data.

Only candidates with a decay length in the XY plane less than 1.5 cm were selected in the analysis to ensure that the vertex was inside the beam pipe, suppressing background caused by interactions in the beam pipe or detector material. The S_l distribution is asymmetric with respect to zero, with charm mesons dominating in the positive tail. Detector resolution effects cause the negative tail, which is dominated by light-flavour events. A smearing [25, 45] was applied to the decay length of a small fraction of the MC events in order to reproduce the negative decay-length data. Finally, a cut $S_l > 4$ was applied; according to MC studies this optimises the statistical precision of the measurement. In addition, the χ^2 of the fitted secondary vertex, $\chi^2_{\mathrm{sec.vtx.}}$, was required to be less than 10 for three degrees of freedom, to ensure good quality of the reconstructed D^+ vertex.

Figure 1 shows the $M(K\pi\pi)$ distribution for the selected D^+ candidates. To extract the number of reconstructed D^+ mesons, the mass distribution was fitted with the sum of a modified Gaussian function for the signal and a second-order polynomial to parametrise the background. The fit function was integrated over each bin. The modified Gaussian function had the form:

$$\mathrm{Gauss}^{\mathrm{mod}} \propto \exp[-0.5 \cdot x^{1+1/(1+\beta\cdot x)}],$$

where $x = |(M(K\pi\pi) - M_0)/\sigma|$ and $\beta = 0.5$. This functional form describes the signals in both the data and MC simulations well. The signal position, M_0, the width, σ, as well as the number of D^+ mesons were free parameters in the fit. The number of D^+ mesons yielded by the fit was $N(D^+) = 8356 \pm 198$. The fitted position of the peak was $M_0 = 1868.97 \pm 0.26\,\mathrm{MeV}$, where only the statistical uncertainty is quoted, consistent with the PDG value of $1869.62 \pm 0.15\,\mathrm{MeV}$ [32].

7 Cross-section determination

For a given observable, Y, the differential cross section in the i^{th} bin was determined as

$$\frac{d\sigma}{dY} = \frac{N^i - N_b^i}{\mathcal{A}_c^i \, \mathcal{L} \, \mathcal{B} \Delta Y^i} \cdot \mathcal{C}_{\text{rad}}^i,$$

where N^i is the number of reconstructed D^+ mesons in bin i of size ΔY^i. The reconstruction acceptance, $\mathcal{A}_c^i$, takes into account geometrical acceptances, detector efficiencies and migrations due to the finite detector resolution. The values of $\mathcal{A}_c^i$ were determined using the RAPGAP MC simulation for charm production in DIS (see Section 4). The quantity $\mathcal{L}$ denotes the integrated luminosity and $\mathcal{B}$ the branching ratio for the $D^+ \to K^-\pi^+\pi^+$ decay channel, which is $9.13 \pm 0.19\%$ [32]. The radiative corrections, $\mathcal{C}_{\text{rad}}^i$, were used to correct measured cross sections to the Born level. For the acceptance determination, the charm MC events were reweighted [25] to reproduce the Q^2, $p_T(D^+)$ and $\eta(D^+)$ distributions in the data.

For all measured cross sections, the contribution of reconstructed D^+ mesons originating from beauty production, N_b^i, was subtracted using the prediction from the RAPGAP MC simulation. This prediction was scaled by a factor 1.6, an average value which was estimated from previous ZEUS measurements [4,46,47] of beauty production in DIS. The subtraction of the b-quark contribution reduced the measured cross sections by 5% on average.

The measured cross sections were corrected to the QED Born level, calculated using a running coupling constant, α, such that they can be directly compared to the QCD predictions by HVQDIS. The RAPGAP Monte Carlo was used to calculate $\mathcal{C}_{\text{rad}} = \sigma_{\text{Born}}/\sigma_{\text{rad}}$, where σ_{rad} is the predicted cross section with full QED corrections (as in the default MC samples) and σ_{Born} was obtained with QED corrections turned off, keeping α running. The corrections are typically $\mathcal{C}_{\text{rad}} \approx 1.02$ and reach 1.10 in the high-Q^2 region.

Figure 2 shows important variables for the secondary-vertex reconstruction, distributions for the DIS variables and the kinematics of the D^+ meson. For all variables, the number of reconstructed D^+ mesons was extracted fitting the number of D^+ mesons in each bin of the distribution. The reweighted MC provides a reasonable description of the data.

8 Systematic uncertainties

The systematic uncertainties were determined by changing the analysis procedure or varying parameter values within their estimated uncertainties and repeating the extraction of the signals and the cross-section calculations. The following sources of systematic uncertainties were considered with the typical effect on the cross sections given in parentheses:

- $\{\delta_1\}$ the cut on the positions $|X|$ and $|Y|$ of the scattered electron in the RCAL was varied by $\pm 1\,\mathrm{cm}$ in both the data and the MC simulations, to account for potential imperfections of the detector simulation near the inner edge of the CAL ($\pm 1\%$);
- $\{\delta_2\}$ the reconstructed electron energy was varied by $\pm 2\%$ in the MC only, to account for the uncertainty in the electromagnetic energy scale ($< 1\%$);
- $\{\delta_3\}$ the energy of the hadronic system was varied by $\pm 3\%$ in the MC only, to account for the uncertainty in the hadronic energy scale ($< 1\%$);
- $\{\delta_4\}$ the FLT tracking-efficiency corrections for the MC (see Section 5) were varied within the estimated uncertainties associated to them ($< 1\%$);
- uncertainties due to the signal-extraction procedure were estimated repeating the fit in both the data and the MC using:
  - $\{\delta_5\}$ an exponential function for the background parametrisation ($< 1\%$);
  - $\{\delta_6\}$ a signal parametrisation changed by simultaneously varying the β parameter of the modified Gaussian function in the data and MC by $^{+0.1}_{-0.2}$ from the nominal value 0.5. The range was chosen to cover the values which give the best description of the mass peaks in the data and MC simulations in bins of the differential cross sections ($^{+0.7\%}_{-1.5\%}$);
- $\{\delta_7\}$ the effect of the decay-length smearing procedure was varied by $\pm 50\%$ of its size, to estimate the uncertainty due to the decay-length description ($\pm 1\%$). As a further cross check, the cut on the decay-length significance was varied between 3 and 5. The resulting variations of the cross sections were compatible with the variation of the decay-length smearing and were therefore omitted to avoid double counting;
- $\{\delta_8\}$ the scaling factor for the MC beauty-production cross sections was varied by ± 0.6 from the nominal value 1.6. This was done to account for the range of the RAPGAP beauty-prediction normalisation factors extracted in various analyses [4,46,47] ($\pm 2\%$);
- the uncertainties due to the model dependence of the acceptance corrections were estimated by varying the shapes of the kinematic distributions in the charm MC sample in a range of good description of the data [25]:
  - $\{\delta_9\}$ the $\eta(D^+)$ reweighting function was varied ($\pm 2\%$);
  - $\{\delta_{10}\}$ the shapes of the Q^2 and $p_T(D^+)$ were varied simultaneously ($\pm 4\%$);
- $\{\delta_{11}\}$ the uncertainty of the pion track inefficiency due to nuclear interactions (see Section 6) was evaluated by varying the correction applied to the MC by its estimated uncertainty of $\pm 50\%$ of its nominal size ($\pm 1.5\%$);
- overall normalisation uncertainties:
  - $\{\delta_{12}\}$ the simulation of the MVD hit efficiency ($\pm 0.9\%$);

- $\{\delta_{13}\}$ the effect of the imperfect description of $\chi^2_{\text{sec.vtx.}}$ was checked by multiplying $\chi^2_{\text{sec.vtx.}}$ for D^+ candidates in the MC simulations by a factor 1.1 to match the distribution in the data (+2%);
- $\{\delta_{14}\}$ the branching ratio uncertainty ($\pm 2.1\%$);
- $\{\delta_{15}\}$ the measurement of the luminosity ($\pm 1.9\%$).

The size of each systematic effect was estimated bin-by-bin except for the normalisation uncertainties ($\delta_{12} - \delta_{15}$). The overall systematic uncertainty was determined by adding the above uncertainties in quadrature. The normalisation uncertainties due to the luminosity measurement and that of the branching ratio were not included in the systematic uncertainties on the differential cross sections.

9 Results

9.1 Cross sections

The production of D^+ mesons in the process $ep \to e' c\bar{c} X \to e' D^+ X'$ (i.e. not including D^+ mesons from beauty decays) was measured in the kinematic range:

$$5 < Q^2 < 1000\,\text{GeV}^2,\ 0.02 < y < 0.7,\ 1.5 < p_T(D^+) < 15\,\text{GeV},\ |\eta(D^+)| < 1.6.$$

The differential cross sections as a function of Q^2 and y are shown in Fig. 3. The cross section falls by about three orders of magnitude over the measured Q^2 range and one order of magnitude in y. The data presented here are in good agreement with the previous ZEUS D^+ measurement[3] [3]. They have significantly smaller uncertainties and supersede the previous results. The NLO QCD predictions calculated in the FFNS, using HVQDIS [23], provide a good description of the measurements. The experimental uncertainties are smaller than the theoretical uncertainties, apart from the high-Q^2 region, where statistics is limited.

Figure 4 shows that the D^+ cross section also falls with the transverse momentum, $p_T(D^+)$, but is only mildly dependent on the pseudorapidity, $\eta(D^+)$. The HVQDIS calculation describes the behaviour of the data well. The results shown in Figs. 3 and 4 are listed in Tables 1 and 2.

Figure 5 shows the differential cross sections as a function of y in five Q^2 ranges. The data are well reproduced by the HVQDIS calculation. The cross-section values are given

[3] The contribution of D^+ mesons from beauty decays was subtracted using the scaled RAPGAP MC predictions.

in Table 3. The effects of individual sources of systematic uncertainties (described in Section 8) on the cross sections in bins of Q^2 and y are given in Table 4.

9.2 Extraction of $F_2^{c\bar{c}}$

The inclusive double-differential $c\bar{c}$ cross section in Q^2 and $x = Q^2/sy$ can be expressed as

$$\frac{d\sigma^{c\bar{c}}}{dx\,dQ^2} = \frac{2\pi\alpha^2}{x\,Q^4}\Big[(1+(1-y)^2)\,F_2^{c\bar{c}} - y^2\,F_L^{c\bar{c}}\Big],$$

where $F_2^{c\bar{c}}$ and $F_L^{c\bar{c}}$ denote the charm contributions to the structure-function F_2 and the longitudinal structure function, F_L, respectively.

The differential D^+ cross sections, $\sigma_{i,\mathrm{meas}}$, measured in bins of Q^2 and y (Table 3), were used to extract $F_2^{c\bar{c}}$ at reference points Q_i^2 and x_i within each bin, using the relationship

$$F_{2,\mathrm{meas}}^{c\bar{c}}(x_i,Q_i^2) = \sigma_{i,\mathrm{meas}}\frac{F_{2,\mathrm{theo}}^{c\bar{c}}(x_i,Q_i^2)}{\sigma_{i,\mathrm{theo}}}, \tag{1}$$

where $F_{2,\mathrm{theo}}^{c\bar{c}}$ and $\sigma_{i,\mathrm{theo}}$ were calculated at NLO in the FFNS using the HVQDIS program. This procedure corrects for the $f(c \to D^+)$ hadronisation fraction and for the extrapolation from the restricted kinematic region of the D^+ measurement ($1.5 < p_T(D^+) < 15\,\mathrm{GeV}$, $|\eta(D^+)| < 1.6$) to the full phase space. The extrapolation factors were found to vary from 1.5 at high Q^2 to 3.0 at low Q^2. The uncertainty on the extrapolation procedure was estimated by applying the same variations that were used to determine the uncertainty of the HVQDIS theoretical predictions (see Section 3) for the ratio $F_{2,\mathrm{theo}}^{c\bar{c}}(x_i,Q_i^2)/\sigma_{i,\mathrm{theo}}$ and adding the resulting ratio uncertainties in quadrature. The procedure of Eq. (1) also corrects for the F_L contribution to the cross section. This assumes that the HVQDIS calculation correctly predicts the ratio $F_L^{c\bar{c}}/F_2^{c\bar{c}}$. This calculation yields a contribution of $F_L^{c\bar{c}}$ between 0% and 3% at low and high y, respectively.

The extracted values of $F_2^{c\bar{c}}$ are presented in Table 5 and Fig. 6. Figure 6 also shows a comparison to a previous ZEUS measurement of $F_2^{c\bar{c}}$ using D^* mesons [2]. The previous results were corrected to the Q^2 grid used in the present analysis using NLO QCD calculations. The two measurements are in good agreement and have similar precision. NLO QCD predictions in the FFNS and GM-VFNS were also compared to the data. The FFNS predictions correspond to the calculations that were used in the $F_2^{c\bar{c}}$ extraction. The GM-VFNS calculations are based on the HERAPDF1.5 [48] PDF set with the charm-quark-mass parameter set to 1.4 GeV. The band shows the result of the variation of the charm-quark-mass parameter from 1.35 GeV to 1.65 GeV in the calculations. Both predictions provide a good description of the data.

9.3 Reduced cross section

The results on D^+ presented here can be combined with other measurements on charm production. Their systematics are largely independent of those using other tagging methods. In such combinations, the quantity used is the reduced charm cross section, defined as

$$\sigma_{\rm red}^{c\bar{c}} = \frac{d\sigma^{c\bar{c}}}{dx\,dQ^2} \cdot \frac{x\,Q^4}{2\pi\alpha^2\,(1+(1-y)^2)} = F_2^{c\bar{c}} - \frac{y^2}{1+(1-y)^2}\,F_L^{c\bar{c}}.$$

The extraction of $\sigma_{\rm red}^{c\bar{c}}$ closely follows the determination of $F_2^{c\bar{c}}$; a modified version of Eq. (1) is used, simply replacing on both sides the structure function by the reduced cross section. The reduced cross sections of the present analysis are corrected to the same Q^2 values as in the charm combination paper of H1 and ZEUS [13] and are presented in Table 6.

10 Conclusions

The production of D^+ mesons has been measured in DIS at HERA in the kinematic region $5 < Q^2 < 1000\,\text{GeV}^2$, $0.02 < y < 0.7$, $1.5 < p_T(D^+) < 15\,\text{GeV}$ and $|\eta(D^+)| < 1.6$. The present results supersede the previous ZEUS D^+ measurement based on a subset of the data used in this analysis. Predictions from NLO QCD describe the measured cross sections well. The charm contribution to the structure-function F_2 was extracted and agrees with that extracted from previous D^* measurements. NLO QCD calculations describe the data well.

The results presented here are of similar or higher precision than measurements previously published by ZEUS. The new precise data provide an improved check of pQCD and have the potential to constrain further the parton densities in the proton.

Acknowledgements

We appreciate the contributions to the construction and maintenance of the ZEUS detector of many people who are not listed as authors. The HERA machine group and the DESY computing staff are especially acknowledged for their success in providing excellent operation of the collider and the data-analysis environment. We thank the DESY directorate for their strong support and encouragement.

References

[1] ZEUS Coll., J. Breitweg et al., Eur. Phys. J. **C 12**, 35 (2000).

[2] ZEUS Coll., S. Chekanov et al., Phys. Rev. **D 69**, 012004 (2004).

[3] ZEUS Coll., S. Chekanov et al., Eur. Phys. J. **C 63**, 171 (2009).

[4] ZEUS Coll., S. Chekanov et al., Eur. Phys. J. **C 65**, 65 (2010).

[5] ZEUS Coll., H. Abramowicz et al., JHEP **11**, 1 (2010).

[6] H1 Coll., C. Adloff et al., Phys. Lett. **B 528**, 199 (2002).

[7] H1 Coll., A. Aktas et al., Eur. Phys. J. **C 51**, 271 (2007).

[8] H1 Coll., F.D. Aaron et al., Phys. Lett. **B 686**, 91 (2010).

[9] H1 Coll., F.D. Aaron et al., Eur. Phys. J. **C 71**, 1769 (2011).

[10] H1 Coll., A. Aktas et al., Eur. Phys. J. **C 45**, 23 (2006).

[11] H1 Coll., F.D. Aaron et al., Eur. Phys. J. **C65**, 89 (2010).

[12] H1 Coll., F.D. Aaron et al., Eur. Phys. J. **C 71**, 1509 (2011).

[13] H1 and ZEUS Coll., H. Abramowicz et al., Submitted to Eur. Phys. J. C. Available at arXiv:hep-ex/1211.1182.

[14] S. Alekhin and S. Moch, Phys. Lett. **B 699**, 345 (2011).

[15] ZEUS Coll., U. Holm (ed.), *The ZEUS Detector*. Status Report (unpublished), DESY (1993), available on `http://www-zeus.desy.de/bluebook/bluebook.html`.

[16] N. Harnew et al., Nucl. Inst. Meth. **A 279**, 290 (1989);
B. Foster et al., Nucl. Phys. Proc. Suppl. **B 32**, 181 (1993);
B. Foster et al., Nucl. Inst. Meth. **A 338**, 254 (1994).

[17] A. Polini et al., Nucl. Inst. Meth. **A 581**, 656 (2007).

[18] M. Derrick et al., Nucl. Inst. Meth. **A 309**, 77 (1991);
A. Andresen et al., Nucl. Inst. Meth. **A 309**, 101 (1991);
A. Caldwell et al., Nucl. Inst. Meth. **A 321**, 356 (1992);
A. Bernstein et al., Nucl. Inst. Meth. **A 336**, 23 (1993).

[19] J. Andruszków et al., Preprint DESY-92-066, DESY, 1992;
ZEUS Coll., M. Derrick et al., Z. Phys. **C 63**, 391 (1994);
J. Andruszków et al., Acta Phys. Pol. **B 32**, 2025 (2001).

[20] M. Helbich et al., Nucl. Inst. Meth. **A 565**, 572 (2006).

[21] J. Smith and W.L. van Neerven, Nucl. Phys. **B 374**, 36 (1992).

[22] B.W. Harris and J. Smith, Phys. Rev. **D 57**, 2806 (1998).

[23] ZEUS Coll., S. Chekanov et al., Phys. Rev. **D 67**, 012007 (2003).

[24] V.G. Kartvelishvili, A.K. Likhoded and V.A. Petrov, Phys. Lett. **B 78**, 615 (1983).

[25] M. Lisovyi, Ph.D. Thesis, Universität Hamburg, Report DESY-THESIS-2011-033, 2011.

[26] ZEUS Coll., S. Chekanov et al., JHEP **04**, 082 (2009).

[27] H1 Coll., F.D. Aaron et al., Eur. Phys. J. **C 59**, 589 (2009).

[28] M. Cacciari, P. Nason and C. Oleari, JHEP **0604**, 006 (2006).

[29] Belle Coll., R. Seuster et al., Phys. Rev. **D 73**, 032002 (2006).

[30] CLEO Coll., M. Artuso et al., Phys. Rev. **D 70**, 112001 (2004).

[31] E. Lohrmann, *A summary of charm hadron production fractions* (unpublished). Available at arXiv:hep-ex/1112.3757, 2011.

[32] J. Beringer et al., Particle Data Group, Phys. Rev. **D 86**, 010001 (2012).

[33] R.G. Roberts and R.S. Thorne, Phys. Rev. **D 57**, 6871 (1998).

[34] G.C. Collins and W.-K. Tung, Nucl. Phys. **B 278**, 934 (1986).

[35] H. Jung, Comp. Phys. Comm. **86**, 147 (1995).

[36] A. Kwiatkowski, H. Spiesberger and H.-J. Möhring, Comp. Phys. Comm. **69**, 155 (1992). Also in *Proc. Workshop Physics at HERA*, eds. W. Buchmüller and G.Ingelman, (DESY, Hamburg, 1991).

[37] CTEQ Coll., H.L. Lai et al., Eur. Phys. J. **C 12**, 375 (2000).

[38] M.G. Bowler, Z. Phys. **C 11**, 169 (1981).

[39] R. Brun et al., GEANT3, CERN-DD/EE/84-1, CERN, 1987.

[40] P.D. Allfrey et al., Nucl. Inst. Meth. **A 580**, 1257 (2007);
W.H. Smith, K. Tokushuku and L.W. Wiggers, *Proc. Computing in High-Energy Physics (CHEP), Annecy, France, Sept. 1992*, C. Verkerk and W. Wojcik (eds.), p. 222. CERN, Geneva, Switzerland (1992). Also in preprint DESY 92-150B.

[41] S. Bentvelsen, J. Engelen and P. Kooijman, *Proc. Workshop on Physics at HERA*, W. Buchmüller and G. Ingelman (eds.), Vol. 1, p. 23. Hamburg, Germany, DESY (1992).

[42] G.M. Briskin, Ph.D. Thesis, Tel Aviv University, Report DESY-THESIS 1998-036, 1998;
ZEUS Coll., J. Breitweg et al., Eur. Phys. J. **C 1**, 81 (1998).

[43] F. Jacquet and A. Blondel, *Proceedings of the Study for an ep Facility for Europe*, U. Amaldi (ed.), p. 391. Hamburg, Germany (1979). Also in preprint DESY 79/48.

[44] V. Libov, A. Spiridonov, private communication.

[45] V. Schönberg, Dissertation, Universität Bonn, Report Bonn-IR-2010-05, 2010, available on `http://hss.ulb.uni-bonn.de/2010/2127/2127.pdf`.

[46] ZEUS Coll., H. Abramowicz et al., Eur. Phys. J. **C 69**, 347 (2010).

[47] ZEUS Coll., H. Abramowicz et al., Eur. Phys. J. **C 71**, 1573 (2011).

[48] H1 and ZEUS Collaborations, *HERAPDF1.5*. Proceedings of the XXXV International Conference of High Energy Physics, Paris, 22–28 July 2010. PoS(ICHEP 2010)168, LHAPDF grid. LHAPDF grid available on `https://www.desy.de/h1zeus/combined_results/index.php?do=proton_structure`.

Q^2 (GeV^2)	$d\sigma/dQ^2$	Δ_{stat} ($\mathrm{nb/GeV}^2$)	Δ_{syst}	$\mathcal{C}_{\mathrm{rad}}$	$d\sigma_b/dQ^2$ ($\mathrm{nb/GeV}^2$)
5 : 10	0.382	± 0.022	$^{+0.027}_{-0.017}$	1.018	0.007
10 : 20	0.150	± 0.007	$^{+0.008}_{-0.010}$	1.016	0.003
20 : 40	0.047	± 0.003	$^{+0.003}_{-0.004}$	1.020	0.002
40 : 80	0.0108	± 0.0008	$^{+0.0008}_{-0.0009}$	1.025	0.0006
80 : 200	0.00192	± 0.00020	$^{+0.00014}_{-0.00016}$	1.042	0.00016
200 :1000	0.000088	± 0.000021	$^{+0.000006}_{-0.000007}$	1.113	0.000013
y	$d\sigma/dy$	Δ_{stat} (nb)	Δ_{syst}	$\mathcal{C}_{\mathrm{rad}}$	$d\sigma_b/dy$ (nb)
0.02: 0.1	16.9	± 0.9	$^{+0.9}_{-0.8}$	1.038	0.1
0.1 : 0.2	13.4	± 0.6	$^{+0.5}_{-0.5}$	1.022	0.3
0.2 : 0.3	8.5	± 0.5	$^{+0.4}_{-0.4}$	1.025	0.3
0.3 : 0.4	6.2	± 0.5	$^{+0.3}_{-0.3}$	1.016	0.3
0.4 : 0.5	4.0	± 0.4	$^{+0.3}_{-0.2}$	1.008	0.2
0.5 : 0.7	2.2	± 0.3	$^{+0.2}_{-0.2}$	0.999	0.2

Table 1: *Bin-averaged differential cross sections for D^+ production in the process $ep \to e' c\bar{c} X \to e' D^+ X'$ in bins of Q^2 and y. The cross sections are given in the kinematic region $5 < Q^2 < 1000\ GeV^2$, $0.02 < y < 0.7$, $1.5 < p_T(D^+) < 15\ GeV$ and $|\eta(D^+)| < 1.6$. The statistical and systematic uncertainties, Δ_{stat} and Δ_{syst}, are presented separately. Normalisation uncertainties of 1.9% and 2.1% due to the luminosity and the branching-ratio measurements, respectively, were not included in Δ_{syst}. The correction factors to the QED Born level, $\mathcal{C}_{\mathrm{rad}}$ are also listed. For reference, the beauty cross section predicted by RAPGAP and scaled as described in the text, σ_b, are also shown.*

$p_T(D^+)$ (GeV)	$d\sigma/dp_T(D^+)$ (nb/GeV)	$\Delta_{\rm stat}$	$\Delta_{\rm syst}$	$\mathcal{C}_{\rm rad}$	$d\sigma_b/dp_T(D^+)$ (nb/GeV)
1.5 : 2.4	2.40	± 0.26	$^{+0.14}_{-0.12}$	1.016	0.07
2.4 : 3	1.44	± 0.12	$^{+0.07}_{-0.05}$	1.020	0.05
3 : 4	1.00	± 0.05	$^{+0.04}_{-0.04}$	1.023	0.03
4 : 6	0.396	± 0.017	$^{+0.014}_{-0.013}$	1.029	0.011
6 : 15	0.0349	± 0.0018	$^{+0.0011}_{-0.0010}$	1.054	0.0011
$\eta(D^+)$	$d\sigma/d\eta(D^+)$ (nb)	$\Delta_{\rm stat}$	$\Delta_{\rm syst}$	$\mathcal{C}_{\rm rad}$	$d\sigma_b/d\eta(D^+)$ (nb)
-1.6:-0.8	1.04	± 0.09	$^{+0.06}_{-0.06}$	1.034	0.02
-0.8:-0.4	1.67	± 0.10	$^{+0.06}_{-0.06}$	1.025	0.05
-0.4: 0.0	1.70	± 0.10	$^{+0.07}_{-0.05}$	1.023	0.05
0.0 : 0.4	1.63	± 0.10	$^{+0.07}_{-0.07}$	1.017	0.06
0.4 : 0.8	1.84	± 0.12	$^{+0.07}_{-0.08}$	1.013	0.06
0.8 : 1.6	1.81	± 0.16	$^{+0.09}_{-0.09}$	1.016	0.05

Table 2: *Bin-averaged differential cross sections for D^+ production in the process $ep \to e' c\bar{c} X \to e' D^+ X'$ in bins of $p_T(D^+)$ and $\eta(D^+)$. Other details are as in Table 1.*

Bin	Q^2 (GeV^2)	y	$d\sigma/dy$	Δ_{stat} (nb)	Δ_{syst}	$\mathcal{C}_{\mathrm{rad}}$	$d\sigma_b/dy$ (nb)
1	5 : 9	0.02 : 0.12	5.46	± 0.59	$^{+0.46}_{-0.30}$	1.026	0.04
2		0.12 : 0.32	3.40	± 0.31	$^{+0.29}_{-0.16}$	1.022	0.06
3		0.32 : 0.7	1.18	± 0.17	$^{+0.10}_{-0.08}$	1.006	0.04
4	9 : 23	0.02 : 0.12	7.02	± 0.45	$^{+0.46}_{-0.49}$	1.028	0.05
5		0.12 : 0.32	3.72	± 0.23	$^{+0.21}_{-0.26}$	1.017	0.09
6		0.32 : 0.7	1.36	± 0.14	$^{+0.09}_{-0.10}$	0.998	0.06
7	23 : 45	0.02 : 0.12	2.84	± 0.27	$^{+0.19}_{-0.22}$	1.040	0.03
8		0.12 : 0.32	1.63	± 0.12	$^{+0.10}_{-0.12}$	1.020	0.05
9		0.32 : 0.7	0.609	± 0.097	$^{+0.047}_{-0.053}$	1.009	0.035
10	45 : 100	0.02 : 0.12	1.14	± 0.18	$^{+0.09}_{-0.10}$	1.046	0.03
11		0.12 : 0.32	0.867	± 0.083	$^{+0.063}_{-0.074}$	1.024	0.050
12		0.32 : 0.7	0.313	± 0.052	$^{+0.032}_{-0.037}$	1.012	0.033
13	100 : 1000	0.02 :0.275	0.560	± 0.085	$^{+0.031}_{-0.038}$	1.117	0.033
14		0.275: 0.7	0.231	± 0.039	$^{+0.020}_{-0.022}$	1.030	0.035

Table 3: *Bin-averaged differential cross sections for D^+ production in the process $ep \to e' c\bar{c} X \to e' D^+ X'$ as a function of y in five regions of Q^2. Other details are as in Table 1.*

Bin	δ_1	δ_2	δ_3	δ_4	δ_5	δ_6	δ_7	δ_8	δ_9	δ_{10}	δ_{11}
1	+6.4% −0.0%	0.0% 0.0%	−0.9% +0.9%	−0.3% +0.3%	+1.3% −0.0%	+0.5% −1.5%	−0.3% +0.3%	+0.9% −0.9%	−3.6% +3.6%	+2.4% −3.1%	+1.7% −1.7%
2	+7.6% −1.8%	−0.1% +0.0%	+0.3% −0.0%	−1.3% +1.3%	+0.1% −0.0%	+0.9% −2.4%	−0.2% +0.2%	+1.4% −1.4%	+0.9% −0.9%	+1.8% −2.3%	+1.6% −1.6%
3	+4.9% −0.0%	+0.2% −0.0%	+0.6% −0.5%	−1.6% +1.6%	+0.5% −0.0%	+1.0% −2.4%	−0.6% +0.6%	+2.2% −2.2%	+5.0% −5.0%	+2.0% −2.6%	+1.6% −1.6%
4	+1.5% −0.0%	0.0% 0.0%	−0.1% +0.3%	−0.2% +0.2%	+2.1% −0.0%	+0.4% −1.0%	−0.1% +0.1%	+0.7% −0.7%	−2.3% +2.3%	+4.8% −6.1%	+1.6% −1.6%
5	−0.6% +0.0%	0.0% 0.0%	−0.1% +0.3%	−1.1% +1.1%	+0.3% −0.0%	+0.8% −2.2%	−0.2% +0.2%	+1.1% −1.1%	+0.4% −0.4%	+4.7% −6.0%	+1.5% −1.5%
6	+0.3% −0.0%	−1.6% +2.2%	−0.2% +0.1%	−1.2% +1.2%	+0.2% −0.0%	+0.7% −1.6%	−1.3% +1.3%	+2.3% −2.3%	+3.7% −3.7%	+3.4% −4.3%	+1.6% −1.6%
7	+0.0% −0.2%	0.0% 0.0%	−0.4% +0.3%	−0.1% +0.1%	+0.6% −0.0%	+0.5% −1.4%	+0.1% −0.1%	+0.8% −0.8%	−2.3% +2.3%	+5.5% −7.1%	+1.5% −1.5%
8	0.0% 0.0%	0.0% 0.0%	−0.2% +0.4%	−0.3% +0.3%	+0.6% −0.0%	+0.1% −0.2%	−0.6% +0.6%	+2.7% −2.7%	0.0% 0.0%	+5.0% −6.5%	+1.3% −1.3%
9	+0.0% −0.6%	−1.5% +1.3%	+1.4% −0.0%	−0.1% +0.1%	−0.6% +0.0%	+0.8% −2.1%	−0.2% +0.2%	+3.7% −3.7%	+2.8% −2.8%	+5.2% −6.7%	+1.5% −1.5%
10	0.0% 0.0%	0.0% 0.0%	−0.9% +0.4%	0.0% 0.0%	+2.7% −0.0%	+0.8% −2.1%	−0.1% +0.1%	+0.9% −0.9%	−1.8% +1.8%	+6.1% −7.8%	+1.3% −1.3%
11	−0.0% +0.1%	0.0% 0.0%	−0.6% +0.4%	0.0% 0.0%	+1.1% −0.0%	+0.2% −0.6%	−0.1% +0.1%	+2.6% −2.6%	−0.3% +0.3%	+6.1% −7.9%	+1.1% −1.1%
12	+0.0% −0.3%	−1.4% +0.2%	+1.0% −0.0%	0.0% 0.0%	+0.4% −0.0%	+0.5% −1.2%	−0.6% +0.6%	+5.2% −5.2%	+2.3% −2.3%	+7.9% −10.1%	+1.3% −1.3%
13	+0.0% −0.5%	0.0% 0.0%	−0.3% +0.7%	0.0% 0.0%	−0.1% +0.0%	+1.3% −3.2%	0.0% 0.0%	+2.6% −2.6%	−1.5% +1.5%	+3.8% −4.9%	+1.0% −1.0%
14	−0.0% +0.1%	−1.2% +0.0%	−1.3% +0.9%	−0.5% +0.5%	+0.2% −0.0%	+0.5% −1.3%	−0.2% +0.2%	+5.5% −5.5%	+0.5% −0.5%	+5.8% −7.5%	+1.0% −1.0%

Table 4: *Contributions of individual sources of systematics for the differential cross sections in bins of y in five ranges of Q^2. The first column gives the bin number that is consistent with Table 3. The systematic variation numbering is consistent with Section 8. Normalisation uncertainties $\delta_{12} - \delta_{15}$ are not shown.*

Q^2 (GeV^2)	x	$F_2^{c\bar{c}}$	Δ_{stat}	Δ_{syst}	Δ_{theo}
6.5	0.00016	0.238	± 0.033	$^{+0.020}_{-0.017}$	$^{+0.033}_{-0.041}$
	0.00046	0.147	± 0.013	$^{+0.013}_{-0.007}$	$^{+0.023}_{-0.013}$
	0.00202	0.073	± 0.008	$^{+0.006}_{-0.004}$	$^{+0.010}_{-0.009}$
20.4	0.0005	0.363	± 0.037	$^{+0.025}_{-0.025}$	$^{+0.032}_{-0.049}$
	0.00135	0.209	± 0.013	$^{+0.012}_{-0.014}$	$^{+0.015}_{-0.013}$
	0.0025	0.170	± 0.011	$^{+0.011}_{-0.012}$	$^{+0.017}_{-0.012}$
35	0.0008	0.377	± 0.060	$^{+0.029}_{-0.033}$	$^{+0.023}_{-0.027}$
	0.0014	0.275	± 0.021	$^{+0.017}_{-0.020}$	$^{+0.016}_{-0.014}$
	0.0034	0.211	± 0.020	$^{+0.014}_{-0.017}$	$^{+0.013}_{-0.020}$
60	0.0015	0.265	± 0.044	$^{+0.027}_{-0.032}$	$^{+0.015}_{-0.013}$
	0.0032	0.212	± 0.020	$^{+0.015}_{-0.018}$	$^{+0.010}_{-0.010}$
	0.008	0.138	± 0.022	$^{+0.010}_{-0.012}$	$^{+0.013}_{-0.009}$
200	0.005	0.215	± 0.036	$^{+0.018}_{-0.021}$	$^{+0.013}_{-0.008}$
	0.013	0.175	± 0.026	$^{+0.010}_{-0.012}$	$^{+0.011}_{-0.008}$

Table 5: *The values of $F_2^{c\bar{c}}$ at each Q^2 and x. The statistical (Δ_{stat}), systematic (Δ_{syst}) and theoretical (Δ_{theo}) uncertainties are given separately. Further uncertainties of 1.9% and 2.1% due to the luminosity and the branching-ratio measurements, respectively, were not included in Δ_{syst}. The theoretical uncertainty, Δ_{theo}, represents the uncertainty due to the extrapolation.*

Q^2 (GeV^2)	x	$\sigma_{\mathrm{red}}^{c\bar{c}}$	Δ_{stat}	Δ_{syst}	Δ_{theo}
			(nb)		
7	0.00016	0.249	± 0.035	$^{+0.021}_{-0.017}$	$^{+0.034}_{-0.043}$
	0.00046	0.155	± 0.014	$^{+0.013}_{-0.007}$	$^{+0.025}_{-0.013}$
	0.00202	0.077	± 0.008	$^{+0.007}_{-0.004}$	$^{+0.011}_{-0.009}$
18	0.0005	0.336	± 0.034	$^{+0.023}_{-0.024}$	$^{+0.029}_{-0.045}$
	0.00135	0.198	± 0.012	$^{+0.011}_{-0.014}$	$^{+0.014}_{-0.012}$
	0.0025	0.161	± 0.010	$^{+0.011}_{-0.011}$	$^{+0.017}_{-0.012}$
32	0.0008	0.352	± 0.056	$^{+0.027}_{-0.031}$	$^{+0.022}_{-0.025}$
	0.0014	0.263	± 0.020	$^{+0.017}_{-0.019}$	$^{+0.015}_{-0.013}$
	0.0034	0.203	± 0.020	$^{+0.013}_{-0.016}$	$^{+0.013}_{-0.019}$
60	0.0015	0.259	± 0.043	$^{+0.026}_{-0.031}$	$^{+0.015}_{-0.013}$
	0.0032	0.211	± 0.020	$^{+0.015}_{-0.018}$	$^{+0.010}_{-0.010}$
	0.008	0.138	± 0.022	$^{+0.010}_{-0.012}$	$^{+0.013}_{-0.009}$
200	0.005	0.210	± 0.035	$^{+0.018}_{-0.020}$	$^{+0.013}_{-0.008}$
	0.013	0.175	± 0.026	$^{+0.010}_{-0.012}$	$^{+0.011}_{-0.008}$

Table 6: *The values of reduced cross sections, $\sigma_{\mathrm{red}}^{c\bar{c}}$, as a function of Q^2 and x. Other details are as in Table 5.*

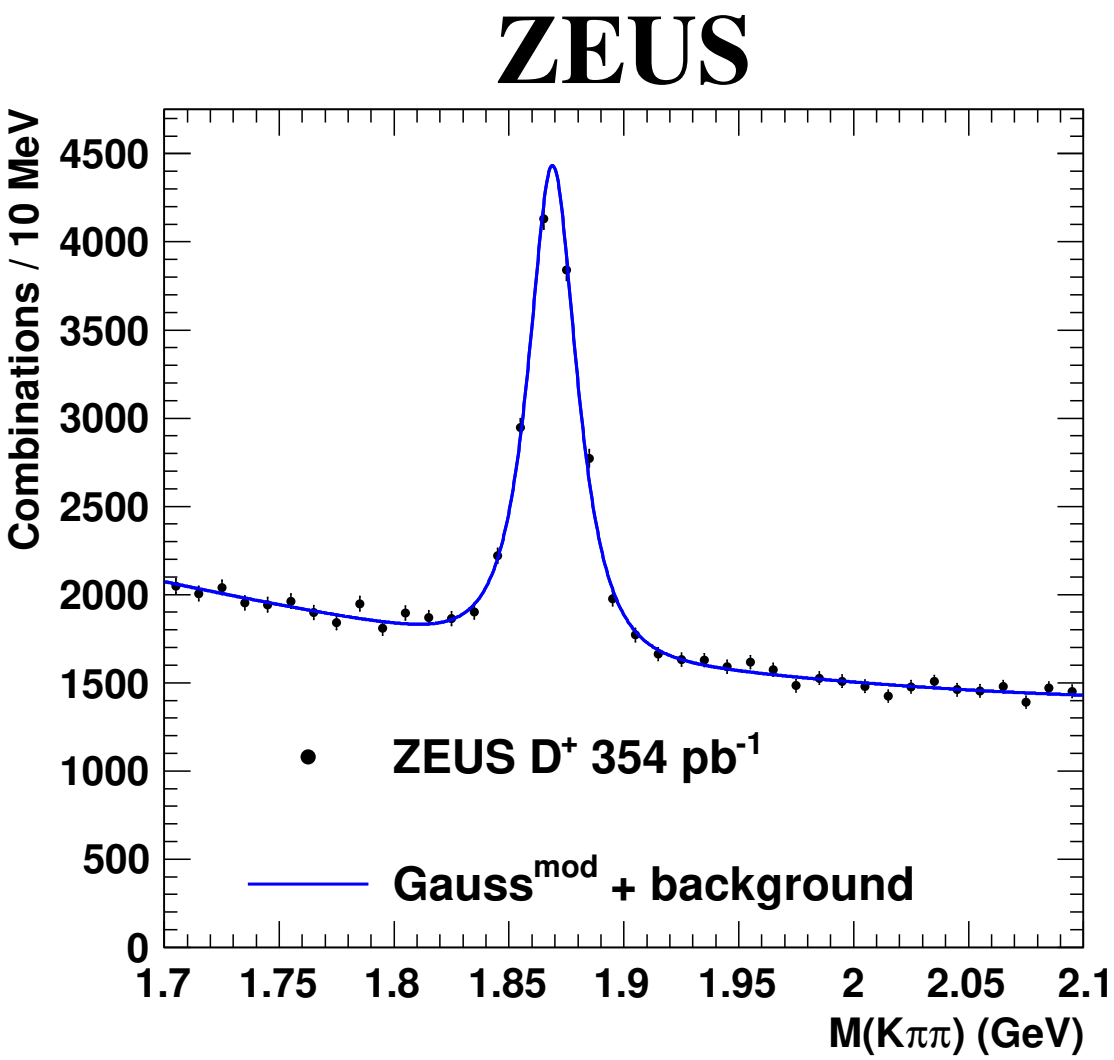

Figure 1: *Mass distribution of the reconstructed D^+ candidates. The solid curve represents a fit by the sum of a modified Gaussian for the signal and a second-order polynomial for the background.*

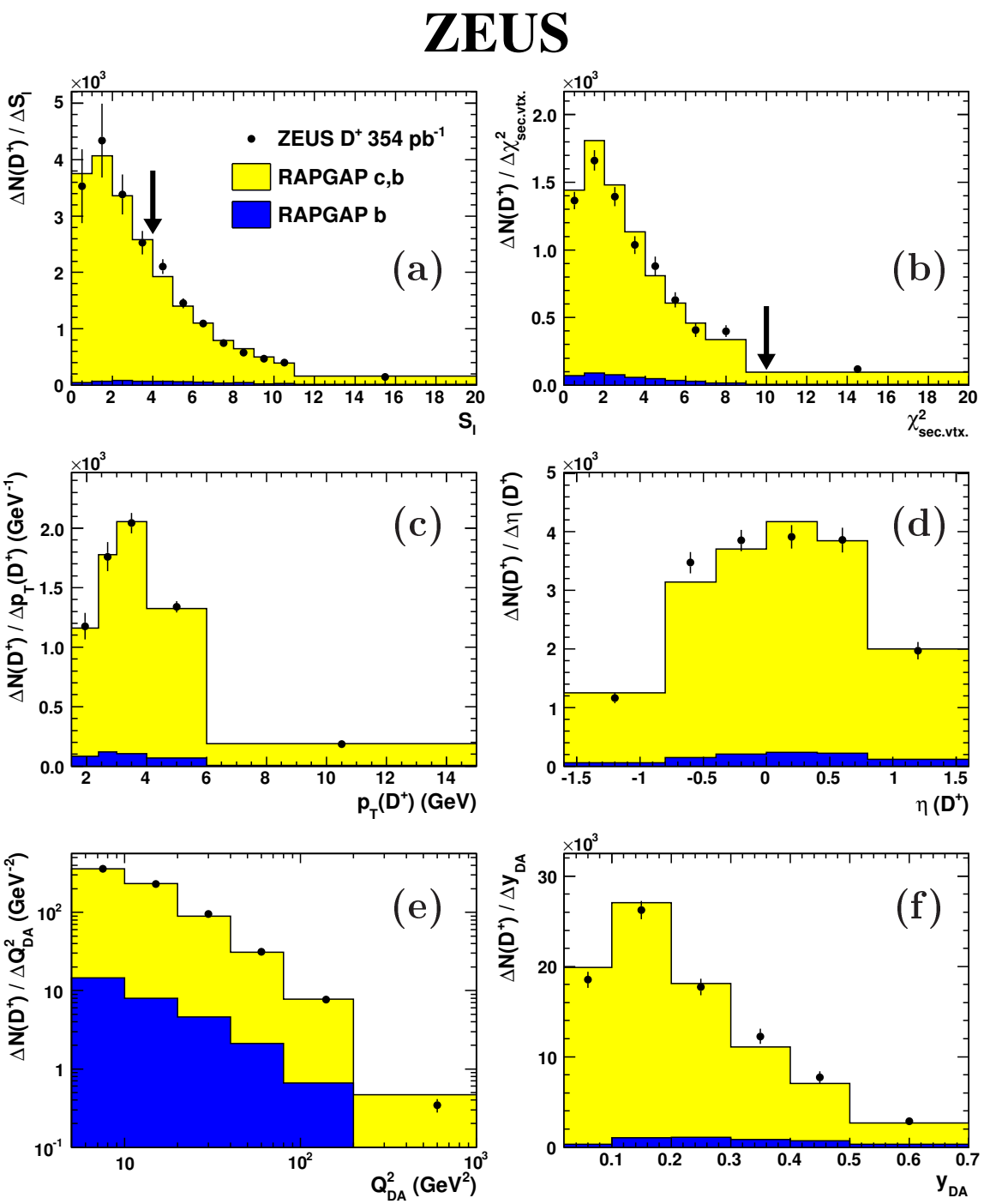

Figure 2: *Bin-averaged differential D^+ distributions of (a) S_l , (b) $\chi^2_{\rm sec.vtx.}$, (c) $p_T(D^+)$, (d) $\eta(D^+)$, (e) $Q^2_{\rm DA}$, (f) $y_{\rm DA}$. The S_l and $\chi^2_{\rm sec.vtx.}$ distributions are shown before the final selection cuts indicated by vertical arrows. The data are shown as black points, with bars representing the statistical uncertainty. Also shown are the simulated charm+beauty MC distributions (light shaded area). The beauty contribution (dark shaded area) is shown separately. The sum of the charm+beauty MC simulations was normalised to the data area.*

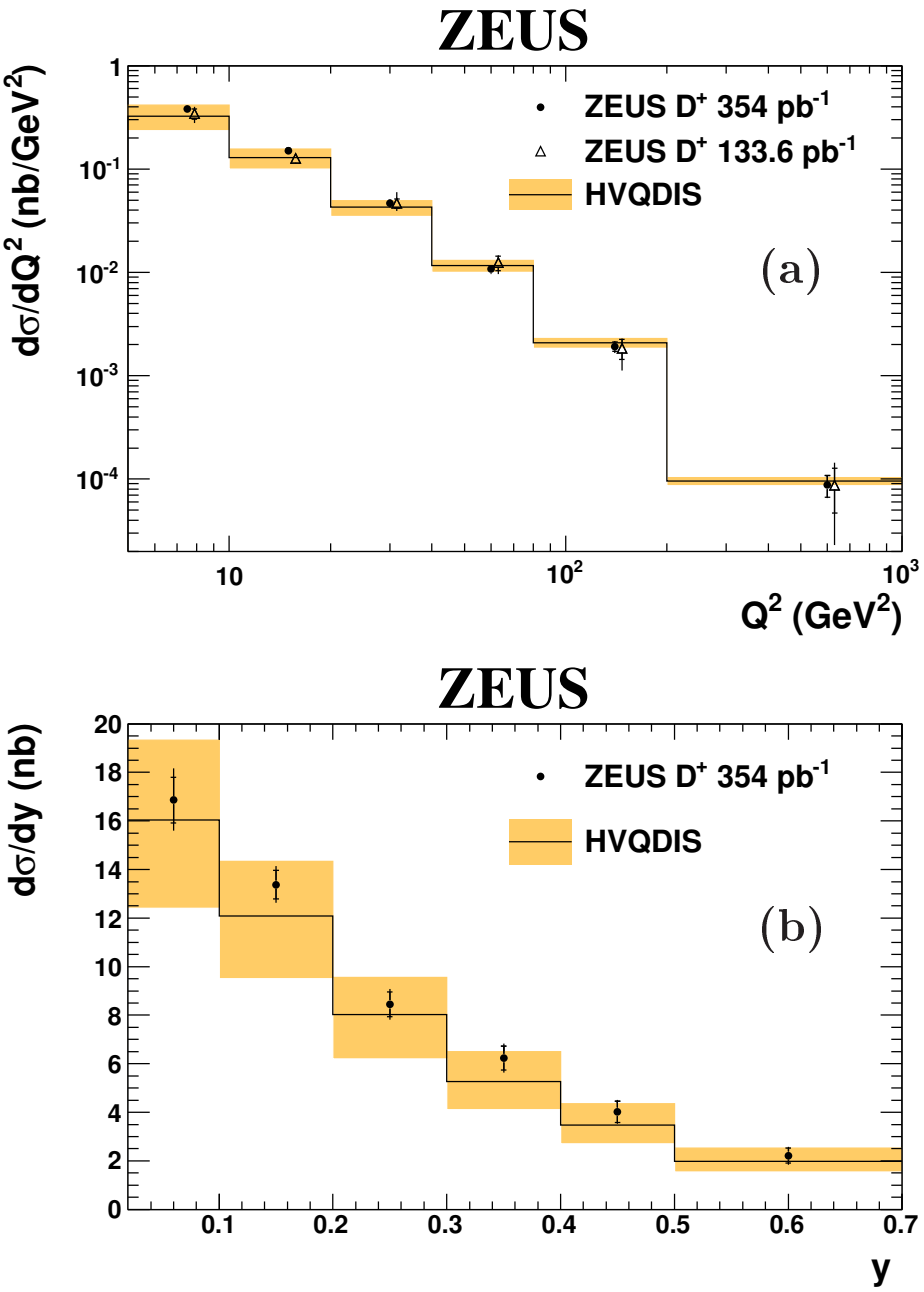

Figure 3: *Bin-averaged differential cross sections for D^+ meson production in the process $ep \to e'c\bar{c}X \to e'D^+X'$ as a function of (a) Q^2 and (b) y. The cross sections are given in the kinematic region $5 < Q^2 < 1000\ GeV^2$, $0.02 < y < 0.7$, $1.5 < p_T(D^+) < 15\ GeV$ and $|\eta(D^+)| < 1.6$. The results obtained in this analysis are shown as filled circles. The inner error bars correspond to the statistical uncertainty, while the outer error bars represent the statistical and systematic uncertainties added in quadrature. For the cross section as a function of Q^2, the results of the previous ZEUS measurement are also shown (open triangles). The solid lines and the shaded bands represent the NLO QCD predictions in the FFNS with estimated uncertainties.*

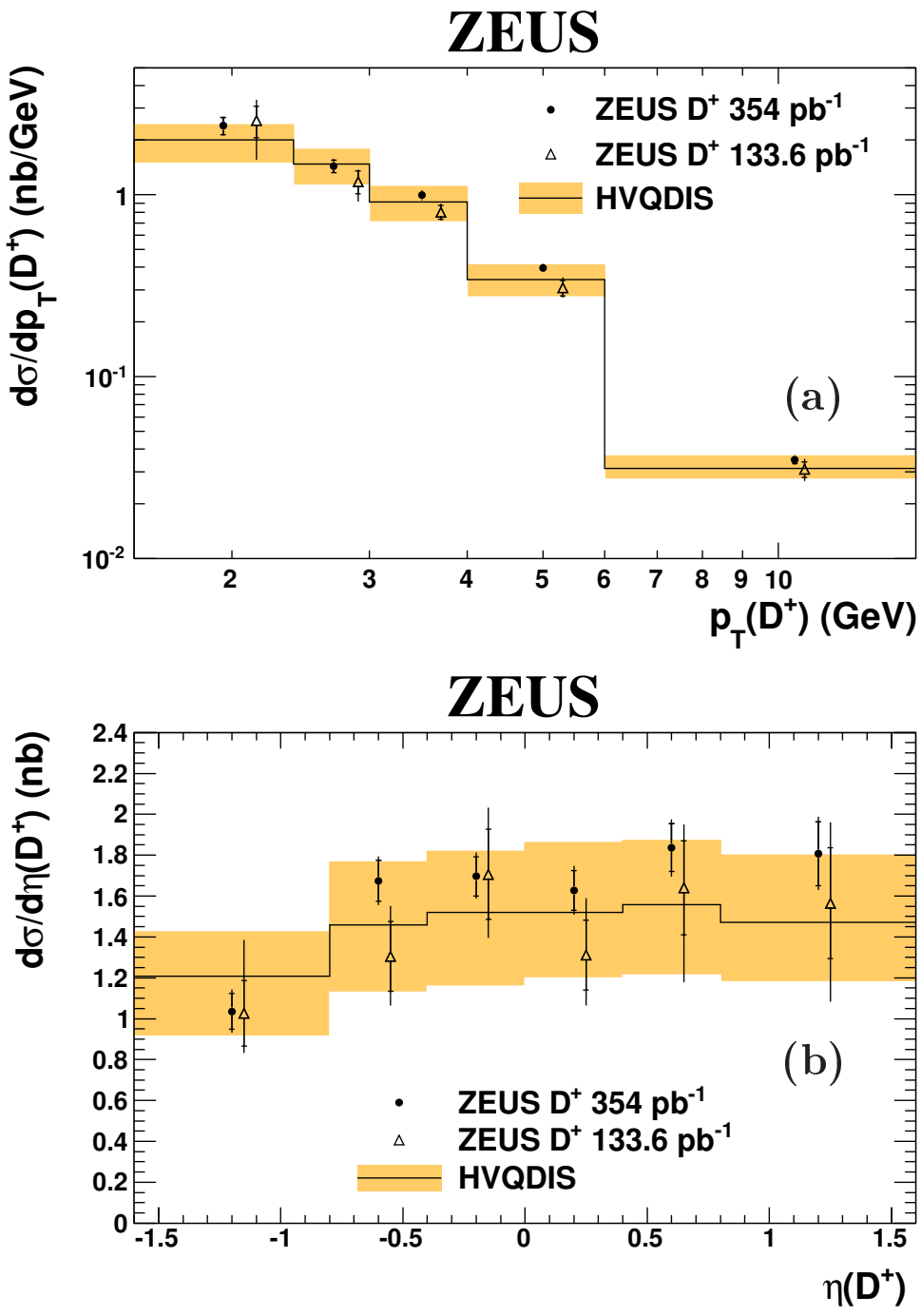

Figure 4: *Bin-averaged differential cross sections for D^+ meson production in the process $ep \to e'c\bar{c}X \to e'D^+X'$ as a function of (a) $p_T(D^+)$ and (b) $\eta(D^+)$. Other details are as in Fig. 3.*

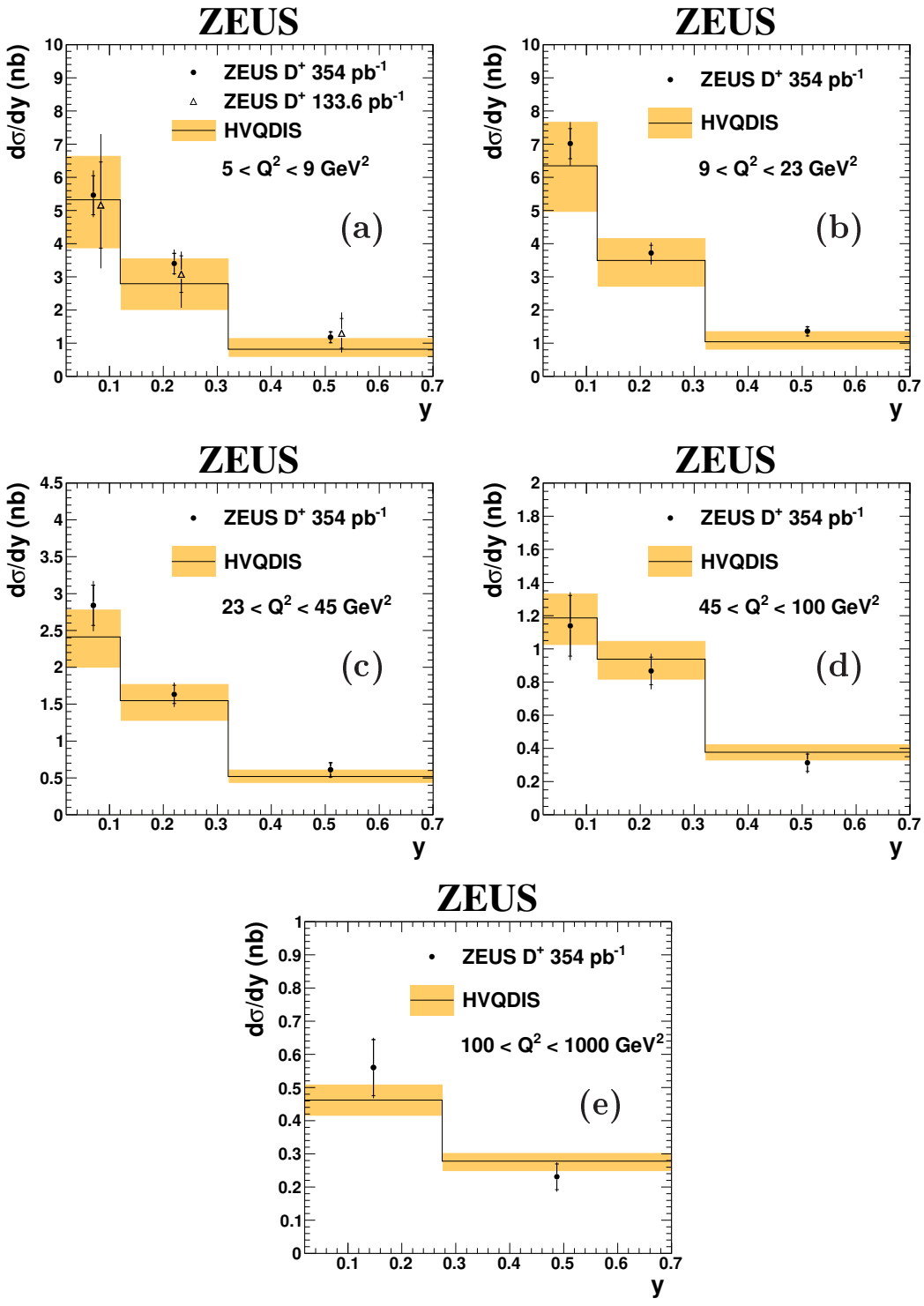

Figure 5: *Bin-averaged differential cross sections for D^+ meson production in the process $ep \to e'c\bar{c}X \to e'D^+X'$ as a function of y in different Q^2 ranges: (a) $5 < Q^2 < 9\ GeV^2$, (b) $9 < Q^2 < 23\ GeV^2$, (c) $23 < Q^2 < 45\ GeV^2$, (d) $45 < Q^2 < 100\ GeV^2$ and (e) $100 < Q^2 < 1000\ GeV^2$. Other details are as in Fig. 3.*

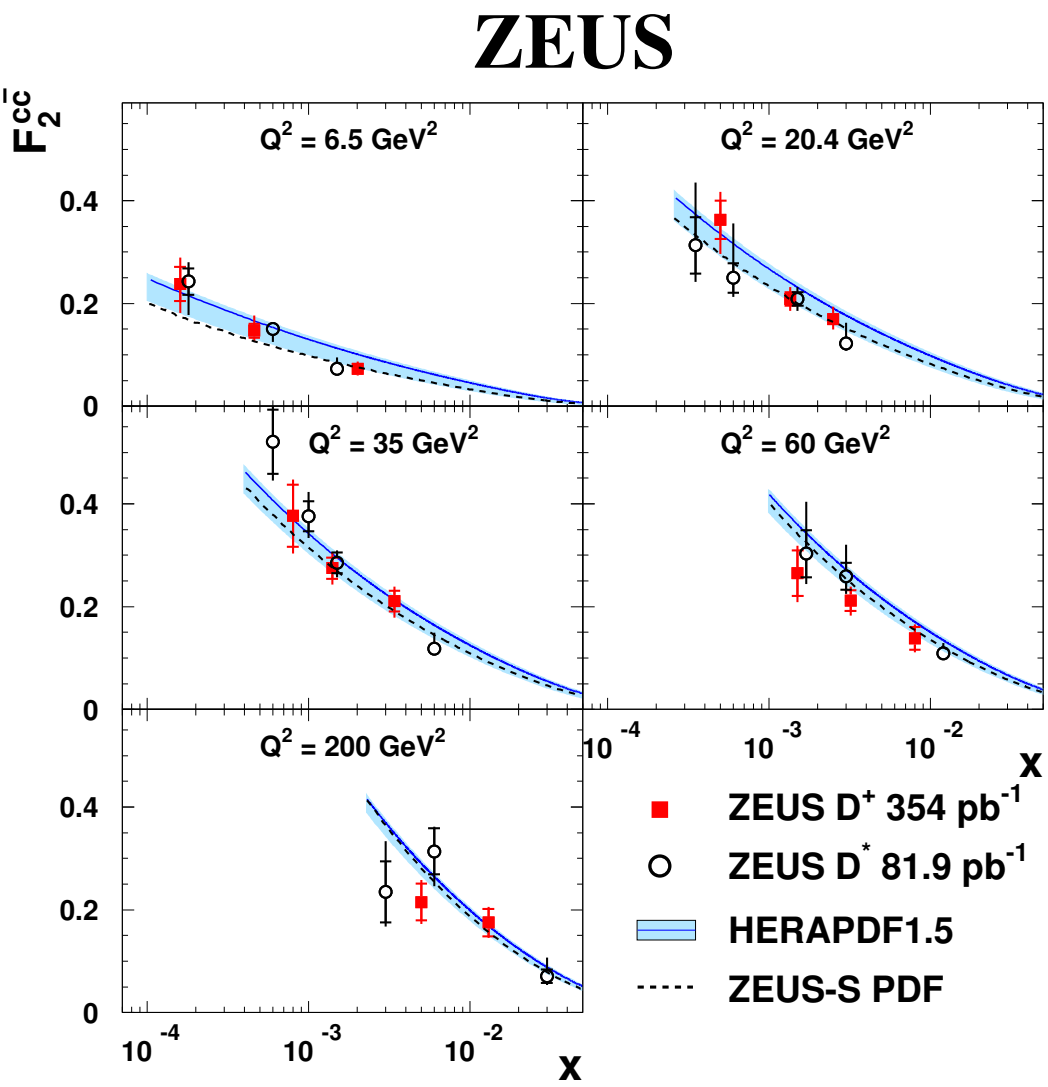

Figure 6: *Structure-function $F_2^{c\bar{c}}$ as a function of x for various values of Q^2. Results obtained in this analysis are shown as filled squares. Also shown are the results of a previous $F_2^{c\bar{c}}$ measurement by ZEUS (open points) based on D^* production. The inner error bars correspond to the statistical uncertainty, while the outer error bars represent the statistical, systematic and theoretical uncertainties added in quadrature. Also shown are predictions in the GM-VFNS based on HERAPDF1.5 with the charm-quark-mass parameter set to 1.4 GeV for the central value (solid line) and its variation in the range 1.35 GeV to 1.65 GeV (filled band). Predictions in the FFNS based on the ZEUS-S PDF set with the default settings described in the text are shown as well (dashed line).*